Original Article

JCBFM

Journal of Cerebral Blood Flow & Metabolism
1–12

DOI: 10.1177/0271678X261437569
journals.sagepub.com/home/jcbfm
Sage

Exploring brain glucose metabolism in multiple sclerosis: A deuterium metabolic imaging study

Alixander S Khan[1], Kamilla Kørup Trosborg[1], Michael Vaeggemose[1,2], Tobias Gaemelke[1], Esben S S Hansen[1], Nichlas Vous Christensen[1], Jack J Miller[1], Rolf F Schulte[3], Caroline Winther Tørring[4,5], Ulrik Dalgas[6], Lars G Hvid[4,6] and Christoffer Laustsen[1]

Abstract

Axonal demyelination is a key feature in multiple sclerosis (MS), that is, increasingly linked to a state of energetic failure, however current non-invasive methods to probe downstream metabolic changes are lacking. This study aimed to investigate Deuterium Metabolic Imaging (DMI) to measure alterations in glucose metabolism in MS compared to healthy controls (HC). In this prospective study DMI was performed on eight patients with relapsing-remitting MS (RRMS) together with eight age- and sex-matched HC. Following oral administration of [6,6′-$^2H_2$] glucose, DMI was acquired on 3 T MRI to quantify the metabolic conversion of glucose (Glc) into glutamate and glutamine (Glx) and lactate. White matter (WM) oxidative metabolism (^{2}H-Glx/^{2}H-Water), showed a negative correlation with the Expanded Disability Status Scale score (EDSS) (Pearson $r = -0.71$, $p = 0.049$). Glucose (^{2}H-Glc/^{2}H-Water), remained unchanged across EDSS (Pearson $r = -0.13$, $p = 0.76$). Impaired glucose levels and oxidative metabolism in WM correlated negatively with increased number of T2-FLAIR lesions (Pearson $r = -0.86$ to -0.83, respectively). These in vivo findings provide evidence for a relative failure of oxidative energy production within the WM of RRMS compared to HC offering proof of concept that DMI is a feasible tool for measuring neurodegeneration related metabolic changes.

Keywords

Metabolism, MRI, multiple sclerosis, MR spectroscopy, X-nuclei

Received 12 November 2025; Revised 17 February 2026; Accepted 13 March 2026

Introduction

Multiple sclerosis (MS) is a neuroinflammatory disease affecting ~2.9 million people worldwide.[1] While advances in treatment have led to the development of effective disease-modifying therapies, there is currently no cure for MS.[2] As a result, both the disease and its symptoms tend to progress over time. Clinical assessment of MS can be made using both clinical tests (such as test of walking capacity, cognitive function, fatigue and composite scores) and magnetic resonance imaging (MRI). Measurement of structural changes in the brain can be measured using fluid-attenuated inversion recovery (FLAIR) sequences where focal lesions can be seen. Alternatively, myelination can be measured using a variety of different MRI techniques such as quantitative susceptibility mapping.[3] Whilst MS severity can be categorised by the Expanded Disability Status Scale (EDSS),[4] to evaluate disability and worsening symptoms, there is a great need for new biomarkers to describe disease progression, characterise patients'

[1]Department of Clinical Medicine, The MR Research Centre, Aarhus University, Aarhus, Denmark
[2]GE HealthCare, Brondby, Denmark
[3]GE HealthCare, Munich, Germany
[4]The Danish MS Hospitals, Ry and Haslev, Denmark
[5]Department of Neurology, Aarhus University Hospital, Aarhus, Denmark
[6]Exercise Biology, Department of Public Health, Aarhus University, Aarhus, Denmark

Corresponding author:
Alixander S Khan, Department of Clinical Medicine, The MR Research Centre, Aarhus University, Aarhus 8000, Denmark.
Email: Ali.Khan@clin.au.dk

symptoms and better understand the mechanism of development.

In relapsing-remitting MS (RRMS) an attack is believed to be caused by an autoimmune inflammatory response against myelin sheaths in the central nervous system (CNS) leading to demyelination, axonal damage and subsequently neurodegeneration.[5] The inflammatory nature of MS fundamentally alters cellular energy demands and metabolic pathway preferences. Activated immune cells (such as microglia and infiltrating lymphocytes) undergo significant metabolic reprogramming, including a pronounced shift towards aerobic glycolysis, to support their rapid proliferation, cytokine production and effector functions during the inflammatory response in MS.[6,7] Likewise, reactive astrocytes exhibit heightened glycolytic activity.[8] This increased glycolytic flux, coupled with potential mitochondrial dysfunction in neurons and oligodendrocytes due to oxidative stress and inflammatory mediators,[9] means that metabolic changes are an important part of the disease.

Metabolic investigations in MS have dated back to the 1950s where altered glucose levels were first reported.[10] Altered metabolism reflects the brain's struggle to meet energy demands in the face of ongoing damage and repair processes as well as reflecting the inflammatory response with activated macrophages opting for highly glycolytic metabolism. The change in metabolism has been linked to disease characteristics[11] and is seen as a potential avenue to expand our understanding of MS. So far, MS research has mainly focussed on systemic glucose stress assessments that have indicated higher anaerobic metabolism in the CNS.[12] More recently, molecular and metabolic imaging can offer improved understanding of the disease. Proton MR spectroscopy has been applied in MS[13–15] showing increased levels of the glutamate pool within the MS brain because of neurodegeneration, however it fails to reflect accumulation information and purely reflects steady-state metabolism. Metabolic changes have also been measured using fluorodeoxyglucose proton emission tomography (FDG-PET) where hypometabolism has been observed within MS[16,17] but reflects only glucose uptake.

Deuterium Metabolic Imaging (DMI) is an emerging metabolic MRI technique providing metabolic information of ^{2}H-labelled glucose's conversion into downstream metabolites. Following the consumption of [6,6′-$^{2}H_2$] glucose, the level of glucose within the brain can be measured alongside downstream metabolic conversion into ^{2}H-lactate and into a combined measurement of labelled glutamate and glutamine, ^{2}H-Glx. The measurement of ^{2}H-Lactate reflects glycolysis, a pathway, that is, typically upregulated in inflammation and cellular stress, whereas ^{2}H-Glx reflects the oxidative phosphorylation (OXPHOS) pathway. In comparison to other metabolic imaging methods such as FDG-PET and hyperpolarised [1-^{13}C] pyruvate MRI, DMI offers a novel measurement of downstream metabolic conversion of glucose with limited technological requirements at lower cost. Moreover, previous applications to brain tumours[18,19] and Alzheimer's disease[20,21] have demonstrated its ability to measure disease related metabolic dysfunction, but its feasibility in measuring MS related changes has yet to be investigated. This study therefore aimed to investigate the feasibility of using DMI to measure alterations in brain glucose metabolism in RRMS patients compared to healthy controls (HC) and establish if measurements correlate with MS disease severity.

Material and methods

Participant characteristics

The research was conducted in accordance with the Declaration of Helsinki and received approval from the Danish Regional Ethical Committee (registration number 1-10-72-51-24). Additionally, the study was preregistered at www.clinicaltrials.gov (identifier: NCT06611280). All participants provided informed consent. Inclusion criteria for RRMS patients were aged between 18 and 60 years, and an EDSS score between 0 and 6.5 (where a limit of 6.5 was set to ensure all patients could enter MRI scanners on their own). Candidates were excluded from participating if they were participating in other clinical trials, were pregnant, had neurological, psychiatric and systemic comorbidities (except hypertension, hyperlipidaemia, atherosclerosis and transient ischaemic attack) or had MR imaging contraindications. No MS patient had suffered from transient ischaemic attacks in this study. One patient was excluded from analysis following imaging due to the impact of a previous brain surgery. For healthy controls to be eligible, they had to meet the same inclusion/exclusion criteria as patients, except those specific for MS. Additionally, they had to match an already enrolled patient on age (±5 years) and sex.

MR imaging

DMI was scanned on a 3 T MRI system (MR750; GE HealthCare) equipped with a volume transmit-receive proton/deuterium head coil (PulseTeq) following fasting for at least 4 h. Participants orally consumed 75 g of [6,6′-$^{2}H_2$] glucose in 200 mL of water and waited at least 60 min before entering the scanner. The subjects entered ~20 min before the ^{2}H-MRSI scan when preparatory scans began. Following acquisition of proton MRI localisers, higher order shimming was performed over an ellipsoid region of the brain using the proton coil. SPGR proton images (inversion time = 450 ms; FOV = 240 mm; TR = 5.4 ms; echo time (TE) = 1.7 ms; flip angle (FA) = 12°; spatial resolution = $0.9 \times 0.9 \times 1\,mm^3$) were acquired to allow for registration to higher resolution proton images. DMI was

acquired following eddy current correction[22] and Bloch–Siegert radiofrequency calibration to adjust transmitted power and resonance frequency.[23] Three dimensional MRSI (real matrix size, $10 \times 10 \times 10$; field of view, $24 \times 24 \times 24\,cm^3$; spectral points, 700; bandwidth, 5000 Hz, flip angle = 70°, TR = 155.8 ms, number of signal averages = 4, total scan time = 17 min and 25 s) was acquired at a mean time of 95 ± 9 min after oral ingestion of D-glucose. Following DMI, the coil was removed and swapped for a 16-channel proton brain coil (GE HealthCare) for high resolution clinical proton imaging consisting of a T1-weighted FSGRE, Neuromix[24] scan for T1 and T2 weighted FLAIR imaging and arterial spin labelling (ASL).

The DMI spectra were reconstructed using the MNS Research Package (GE HealthCare), denoised with tMP-PCA[25,26] using multiple signal averages, partial volume corrected and bias field corrected using MICO[27] in MATLAB 2024b. For quantification, the DMI spectra were fit voxel-wise using OXSA-AMARES.[28] The resulting maps of deuterated water, glucose, lactate and Glx were then linearly interpolated to the resolution of the anatomical images for visual overlays. For regional analysis, anatomical T_1-weighted images were segmented using SPM12[29] to segment the brain into three "brain" compartments, grey matter (GM), white matter (WM) and cerebrospinal fluid (CSF) and one "background" compartment containing all voxels that were not identified as the above. To quantitatively analyse DMI data from these compartments, the Spectroscopy with Linear Algebraic Modelling (SLAM) approach[30] was used to produced spatially localised spectra that effectively come from the non-rectilinear compartments denoted above. SLAM effectively incorporates prior information, in the form of these binary masks corresponding to anatomically segmented proton 3D localiser images, into the reconstruction of phase-encoded MRSI data, giving one spectrum per anatomical segment.[30–32] Compartmentalised spectroscopy approaches effectively adjust the spectral response function of the CSI acquisition to become shaped like the target segmented volume of interest, and therefore effectively swap having a larger number of regularly spaced voxels for a smaller number of irregularly spaced voxels with a typically better full-width-half-maximum spectral response function along anatomically meaningful contours of interest. They have been extensively validated against higher resolution prospectively acquired CSI data and are routinely used in the context of phosphorus[33,34] and proton[35] spectroscopy. The spatial response function for the individual tissue maps was simulated to highlight the ability of SLAM to resolve distinct compartments and shape the appropriate SRF to anatomically meaningful regions (Supplementary Materials Figure 1(a)). After reconstruction, the individual tissue's spectra were produced which were subsequently fit using OXSA–AMARES to produce metabolic values for each tissue. Correlation analysis between SLAM and segmentation of OXSA–AMARES fitted maps are shown in Supplementary Materials Figure 1(b).

Following quantification, metabolic ratios of ^{2}H-Glc and ^{2}H-Glx to the naturally abundant ^{2}H-Water peak were taken, reflecting the level of glucose within the blood stream and the oxidative metabolism, respectively. Values were not corrected for T_1.

Segmentation of FLAIR images was performed using Lesion Segmentation Tool (LST)[36] in SPM12 to extract lesion volume and total number of lesions.

Clinical tests

Blood glucose and lactate levels were measured in a resting state before ingestion of the deuterated glucose from a 100 µL capillary blood sample and analysed using the ABL90 Flex Plus arterial blood gas sampling system (Radiometer Medical ApS, Denmark).

Physical function was assessed by three separate walking tests and the 5-time sit-to-stand test (5STS). The following tests assessed walking capacity and were performed in order: (1) The timed 25-foot walk test (T25FWT) measured maximal walking speed. The test was performed twice and expressed as a two-trial average in m/s.[37,38] (2) The six spot step test (SSST) measured walking balance/coordination. The test was performed twice for each leg and expressed as a four-trial average completion time.[39] (3) The 6-min walk test (6MWT) measured walking endurance expressed in meters.[40] Finally, the 5STS test assessed chair-raising ability in terms of the time taken to complete five sit to stand movements from a chair. The test was performed twice and expressed as a two-trial average completion time.[41]

Cognitive function was assessed using the selective reminding test (SRT) and symbol digit modalities test (SDMT). The SRT measured memory from long-term storage, consistent long-term storage and 20-min delayed recall; all SRT outcomes are expressed as the number of correct words recalled.[42] The SDMT measured cognitive processing speed and attention by having participants translate geometric symbols into numbers. The test score was the number of correct translations in 90 s.[43]

Two patient-reported outcome measures were administered. First, the modified fatigue impact scale (MFIS) assessed the subjective perception of fatigue impact, where a higher score indicates more fatigue impact.[44] Second, the MS impact scale (MSIS) assessed the impact of MS on the life of a MS patient.[45] The MSIS questionnaire was only given to participants with MS. A higher score indicated a greater impact of the disease on daily functioning.

EDSS scores were obtained from their medical records (and determined within 6 months of imaging). Patients were grouped into low and moderate severity groups based on their EDSS score. An EDSS score of 2.5 was set as the threshold to separate low disease severity ($n = 3$) and moderate disease severity ($n = 5$).

Table 1. Cohort characteristics. Data are presented as mean ± SD and ranges in brackets, $n = 3$ patients had an EDSS score ⩽2.5.

Participant group	Healthy controls	MS
Age (years)	38 ± 10 (26–52)	39 ± 10 (25–53)
Sex	5F:3M	5F:3M
Physical tests		
Six-min walk test (m)	614 ± 84 (514–750)	493 ± 174 (203–717)
Six spot step test (s)	5.6 ± 0.7 (4.7–6.6)	7.9 ± 3.3 (4.0–12.6)
5× Chair raise (s)	7.8 ± 2.5 (5.2–11.5)	13.2 ± 7.7 (5.6–26.2)
MFIS		
Physical subscale (0–36)	2 ± 3 (0–8)	14 ± 8 (2–26)
Cognitive subscale (0–40)	6 ± 5 (1–16)	16 ± 9 (2–25)
MSIS		
Physical impact score (20–80)		38.0 ± 23.7 (1.25–56.25)
Psychological impact score (9–36)		35.8 ± 18.8 (2.7–58.3)
Cognitive		
Selective reminding test	57.6 ± 8.7 (40–68)	40.9 ± 11.2 (26–62)
Symbol digit modality test	59.5 ± 9.3 (47–79)	43.3 ± 19.0 (20–72)

MFIS: Modified Fatigue Impact Scale, MSIS: Multiple Sclerosis Impact Scale.

Statistics

Statistical analyses were performed using GraphPad Prism (v10.4.1), and a $p < 0.05$ was considered significant. Data distribution was assessed for normality using the Kolmogorov-Smirnov test.

Initial between-group comparisons (MS patient vs healthy controls) of metabolic ratios within different tissue types were performed using unpaired unequal variance Student's *t*-test or the Mann–Whitney *U* test, as appropriate. Assessment of cerebral tissue changes within cohorts used paired *t*-tests. To investigate the relationship between metabolic ratios and clinical measures (e.g. EDSS, lesion burden, functional tests), simple linear regression was used to determine the coefficient of determination (R^2) and to test if the slope was different from zero.

To create a composite metric of overall physical function, a physical *Z*-score was calculated by averaging the standardised scores of the 6MWT, SSST and 5STS and dividing by the standard deviation of the HC group.

Finally, two-way repeated measures ANOVA was employed to test for main effects and interaction effects between disease severity subgroups (healthy controls, low EDSS, moderate EDSS) and tissue compartments (e.g. GM, WM, CSF).

Results

Participant characteristics

The present study employed a cross-sectional design that included nine participants with relapse-remitting MS (RRMS; three males and six females, mean age: 39 ± 10 years) with a broad distribution of EDSS scores (min = 0, max = 6.5/10, mean = 3 ± 2) and eight healthy controls (three males and six females, mean age: 38 ± 10 years). A final cohort of eight MS patients and eight healthy controls was included in the analysis (Table 1). The groups were well-matched for age and sex. As expected, patients demonstrated poorer performance on average across all physical and cognitive tests compared to controls.

Initial group comparisons reveal no global metabolic changes

Initial group-wise comparisons of DMI metabolic ratios did not reveal any significant differences between MS patients and HC in either WM or GM (Figure 1).

Metabolic changes with disease severity

Disease based changes were investigated by looking at the relationship between metabolic ratios and the EDSS score in the WM. Whilst ^{2}H-Glc/^{2}H-Water did not show any correlation with EDSS score ($p = 0.76$, Pearson $r = -0.12$; Figure 2(a)), ^{2}H-Glx/^{2}H-Water showed a significant negative correlation ($p = 0.048$, Pearson $r = -0.71$; Figure 2(a)). We also investigated the relation between WM and GM metabolism in the HC and MS cohorts where we observed only the MS patients showed significant differences in ^{2}H-Glx/^{2}H-Water between the WM and GM (HC: GM = 0.25 ± 0.08, WM = 0.24 ± 0.06, MS: GM = 0.30 ± 0.09, WM = 0.23 ± 0.09, $p < 0.0001$; Figure 2(b)).

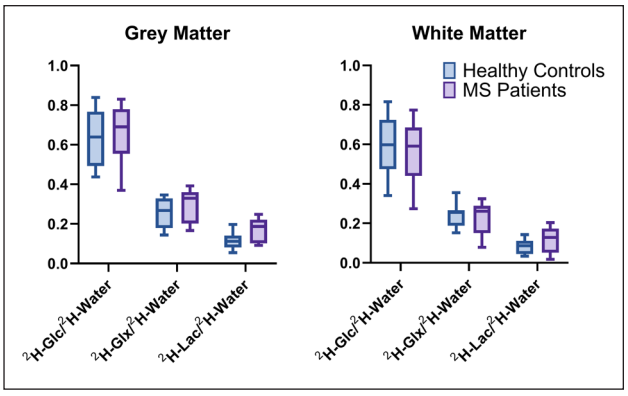

Figure 1. Group wise comparison between patients and HC across the entire cohort. Error bars represent 10th–90th percentile. No significant differences were seen in brain metabolism either across the whole brain or within tissue types.

Metabolic differences categorised by disease severity

We next categorised patients based on their EDSS score to stratify MS severity and investigated how metabolism changes in different tissue types and disease severity subgroups ($n=8$: healthy controls, $n=3$: low EDSS ($\leqslant 2.5$) and $n=5$: moderate EDSS (>2.5)). Patient characteristics of the two MS groups are shown in Supplementary Table 1. All subjects showed a trend of decreased ^{2}H-Glc/^{2}H-Water within the WM compared to GM (Figure 2(c); HC: $p=0.05$, low MS: $p=0.003$, moderate MS: $p=0.014$). However, only the MS group showed trends of decreased ^{2}H-Glx/^{2}H-Water within the WM compared to the GM, with the moderate MS group with the most significant decrease in the WM (Figure 2(c); HC: $p=0.31$, low MS: $p=0.012$, moderate MS: $p=0.0002$).

When repeating the analysis for the HC group and grouping the cohort based on their age matched patients EDSS score (to create a "low" and "moderate" matched severity group), no correlations were found implying that metabolic changes were not a consequence of age or sex.

MRSI maps of ^{2}H-Glx/(^{2}H-Glc + ^{2}H-Water) shown in Figure 3 illustrate differences between the three groups with representative images taken from HC, MS patients with low severity (EDSS = 0) and MS patients with moderate severity (EDSS = 4.5 and 6.5). Spectra extracted from the WM region using SLAM analysis illustrates the decreased ^{2}H-Glx peak within the moderate severity group, fitted spectra is provided in the Supplementary Materials Figure 3.

Metabolic changes related to structural and functional impairment

As a further marker of MS severity, metabolic changes because of cerebral lesions was investigated. Initial

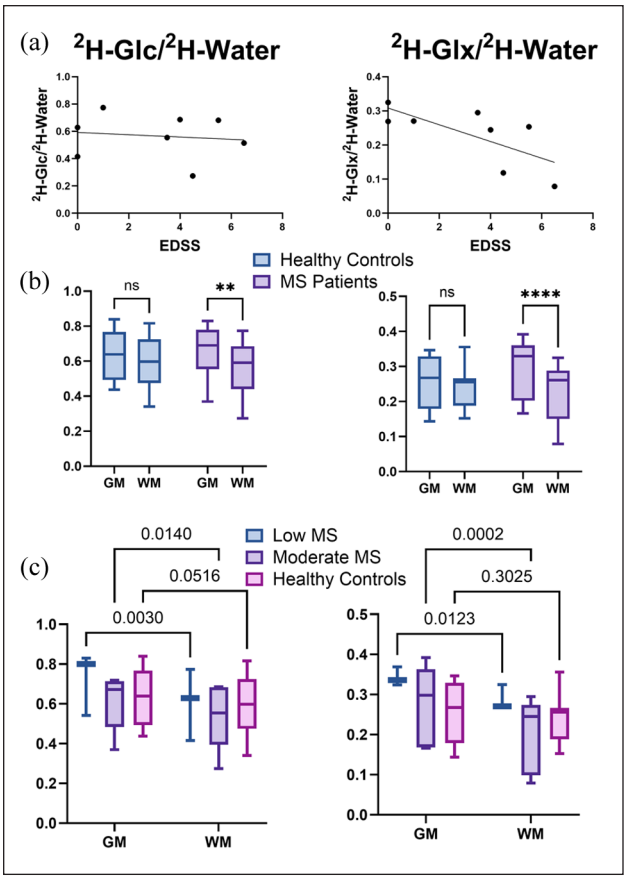

Figure 2. Metabolic changes with disease severity shows changes both within the WM and relative to the GM: (a) the level of ^{2}H-Glc/^{2}H-Water remains the same across EDSS severity within the WM ($p=0.76$, Pearson $r=-0.12$), however, ^{2}H-Glx/^{2}H-Water showed a negative correlation as EDSS severity increases within the WM ($p=0.048$, Pearson $r=-0.71$), (b) comparison between the GM and WM showed that only the MS cohort showed significant changes between the cerebral tissues, potentially owing to increased cellular damage in the WM making changes more pronounced (**$p \leqslant 0.01$, ***$p \leqslant 0.001$), and (c) classifying MS patients based on EDSS score (low EDSS ($\leqslant 2.5$, $n=3$), moderate EDSS (>2.5, $n=5$)) showed that the GM to WM change became more pronounced in the more severe MS cohort.

segmentation analysis to assess lesion metabolism showed no significant changes compared to the normal appearing brain (Supplementary Materials Figure 2) likely due to the low volume of the lesions. However, we investigated the correlation of metabolic change to lesion volume and total number of lesions as a marker of lesion burden and structure damage. Lesion volume was found to be predominately located in the WM (ratio of lesion volume in GM/ lesion volume in WM: 0.25 ± 0.16). Lesion volume correlated significantly with impaired glucose metabolism (^{2}H-Glc/^{2}H-Water) and showed trends with oxidative metabolism (^{2}H-Glx/^{2}H-Water) in the white matter ($p=0.016$, $r=-0.8$, $p=0.11$, $r=0.61$, respectively; Figure 4(a) and (b)).

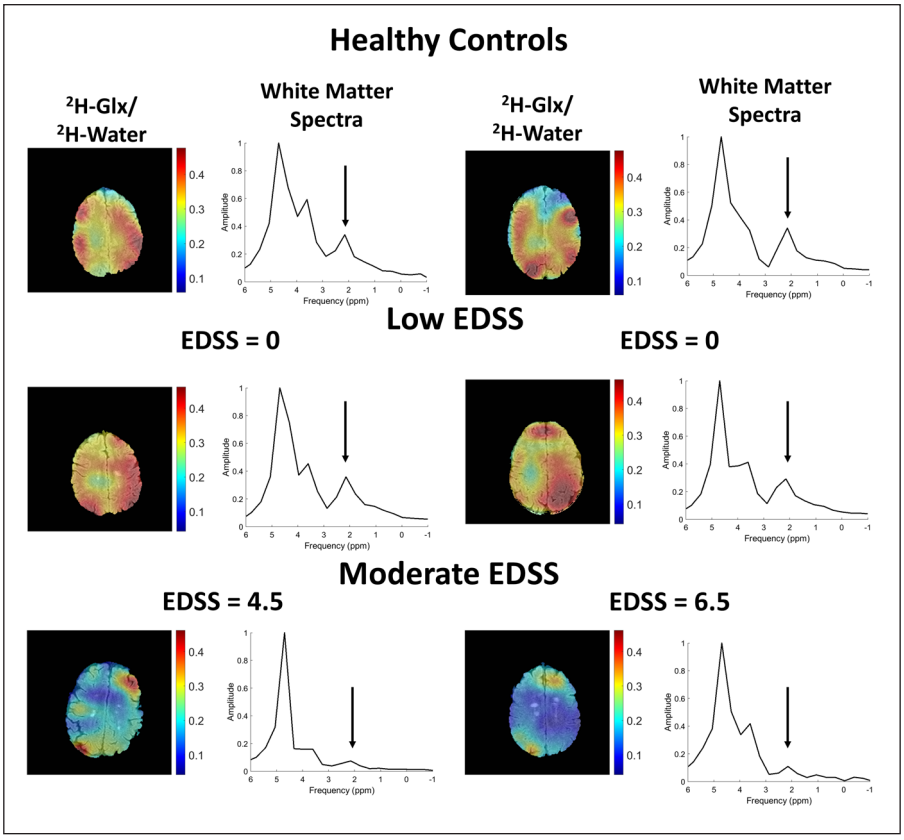

Figure 3. Interpolated metabolic maps of ^{2}H-Glx/^{2}H-Water in two healthy control participants (lesion volume = 0.1 and 0.7 mL, number of lesions = 4 and 12), two MS patients with low severity (EDSS = 0, lesion volume = 2 and 0.18 mL, number of lesions = 21 and 5) and two MS patients with high severity (EDSS = 4.5, 6.5, lesion volume = 24 and 5.26 mL, number of lesions = 31 and 26). Spectra extracted from all voxels within the white matter using SLAM is shown with the Glx peak highlighted.

However, the high lesion volume outlier (24.4 mL) had a high leverage and high Cook's distance from the other subjects and when removed significance is lost. As an alternative measure of lesion burden, the number of lesions was found to be significantly associated with metabolic changes within the WM. Decreases in both ^{2}H-Glc/^{2}H-Water and ^{2}H-Glx/^{2}H-Water with increasing number of lesions were measured in the WM ($p = 0.0056$, $r = -0.86$, $p = 0.011$, $r = -0.83$, respectively) Lesion burden itself was not significantly correlated with EDSS (Supplementary Materials Figure 4).

Composite *Z*-scores were found from physical performance tests where higher *Z*-scores corresponded to improved physical performance compared to the rest of the cohort. The metabolic changes were compared to patient function, where a higher ^{2}H-Glx/^{2}H-Water within the WM showed trends of relation with better overall physical performance, as measured by a composite physical *Z*-score ($p = 0.12$, $r = 0.6$; Figure 5). However, comparison to cognitive performance tests, MFIS cognitive surveys and SDMT did not show any correlation.

Discussion

In this study we investigated the feasibility of measuring changes of downstream metabolism in MS using DMI. We observed that in our cohort decreased levels of ^{2}H-Glx/^{2}H-Water correlated with disease severity within the WM. Interestingly however, ^{2}H-Glc/^{2}H-Water did not show significant changes as EDSS increased. Whilst overall group level changes were not observed, our patient cohort was heterogenous covering early onset MS with little to no symptoms to more severe symptomatic MS. A significant decrease in ^{2}H-Glc/^{2}H-Water and ^{2}H-Glx/^{2}H-Water within the WM relative to the GM was seen only in MS patients compared to the HC cohort. This pilot investigation acts as a proof of concept for further studies to investigate downstream metabolic change in MS.

Disease severity was also quantified by lesion burden, physical function, cognitive function and fatigue. Whilst physical function showed modest trends and cognitive function and fatigue did not correlate with metabolic changes, lesion burden was found to relate to metabolism.

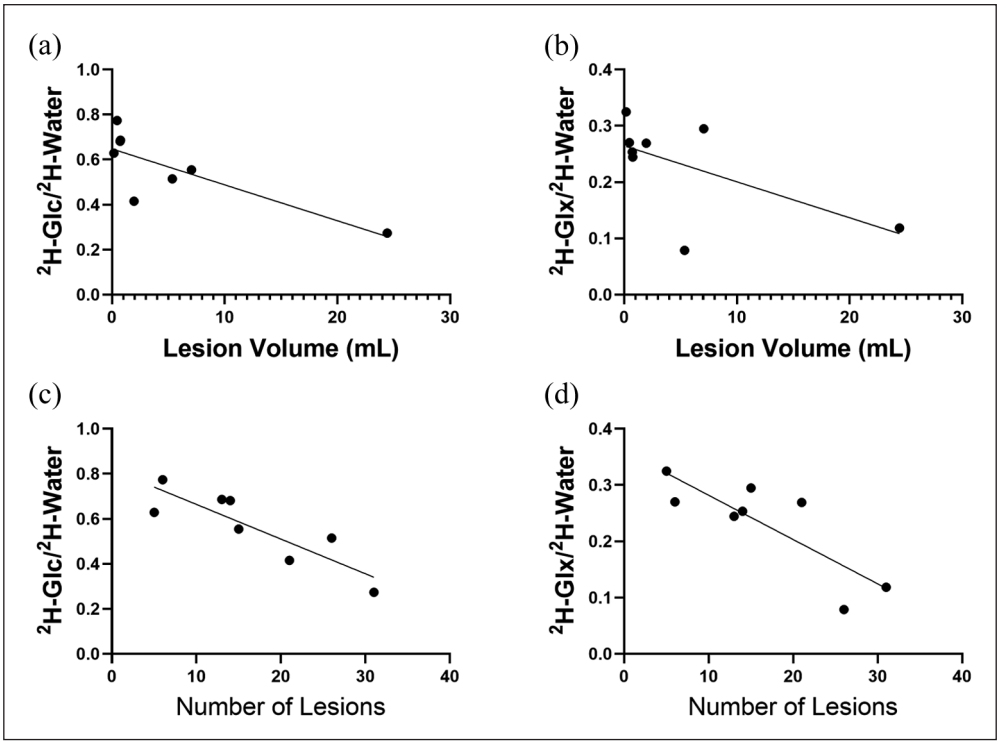

Figure 4. Relationship between metabolism and lesion burden: (a) decreased glucose metabolism and (b) oxidative metabolism correlated with increasing lesion volume in the white matter. As an alternative measure of lesion burden, the total number of lesions was investigated which also correlated with decreases in (c) glucose metabolism and (d) oxidative metabolism within the white matter.

Whilst EDSS, lesion burden and physical performance are all closely related,[46,47] each measurement reflects a different domain of disability that may reflect different patients' experiences. Lesion burden showed an inverse relation with both ^{2}H-Glc/^{2}H-Water and ^{2}H-Glx/^{2}H-Water in the WM, where both hypometabolism and impaired oxidative metabolism was observed with increasing lesion burden. Whilst, physical function showed trends of relation to WM oxidative metabolism, cognitive function did not show any relation, potentially owing to the limited sensitivity of DMI.

An interesting observation is the diverging between the correlations of EDSS to metabolism and lesion burden. Whilst lesion burden showed both decreased overall ^{2}H-Glucose levels (measured as ^{2}H-Glc/^{2}H-Water) and impaired oxidative metabolism (measured with ^{2}H-Glx/^{2}H-Water), ^{2}H-Glucose levels were relatively unchanged across disease scales. This potentially reflects the different measurements made with lesion load and EDSS score, one reflecting structural damage to the brain, and likely local perfusion loss, the other clinically derived from patient symptoms. Hypometabolism because of MS has previously been shown to occur using FDG-PET, where whole brain and lesion specific decreases in glucose uptake was seen.[16,17] Whilst we could not individually segment lesions, the WM based changes we observe support this.

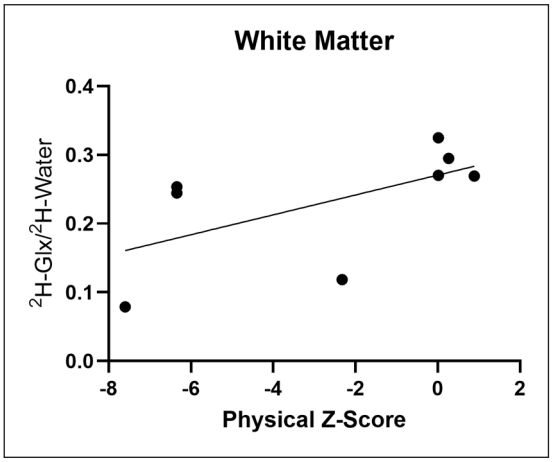

Figure 5. Correlation of physical *Z*-score to ^{2}H-Glx/^{2}H-Water within the white matter showed trends of increased physical performance related to increased oxidative metabolism (Pearson $r = 0.59$, $p = 0.12$).

The measurement of ^{2}H-Glc levels remaining the same with disease severity but with impaired oxidative metabolism reflects the potential utility of DMI. Whilst ^{2}H-Glc/^{2}H-Water reflect blood glucose levels within brain, and act as a marker of overall delivery, ^{2}H-Glx/^{2}H-Water offers a more sensitive measure of cellular change which may be

more disease driven. Indeed, unlike FDG-PET, where the glucose becomes trapped within the intracellular compartment, ^{2}H-Glc is likely to exist primarily within the blood, where any uptake into the cells is metabolised to downstream products.

Metabolic dysfunction is a key driver of the pathogenesis in MS having a role in the neuroinflammation process that subsequently causes neurodegeneration. The primary event is the infiltration of immune cells which attack the myelin sheath within the WM and leads to a cascading effect. As a result of demyelination, redistribution of ion channels[48] must occur which increases the ATP demand,[49] subsequently leading to an increased density of functional mitochondria within the area of demyelination.[50] However, because of activated microglial generating reactive oxygen species[51] and the products of inflammation,[52] mitochondrial function becomes impaired,[53,54] further impairing axonal function. In parallel, oligodendrocytes, playing a vital role in maintaining myelin integrity, typically already operating under aerobic glycolysis and continue to shift towards greater glycolytic metabolism for survival in the presence of inflammation.[55,56] The combined effects of this widespread energy failure are shown in and push the system to a metabolic shift where activated immune cells opt for aerobic glycolysis[57,58] to compensate for the changes. As the disease progresses, increased impairment of metabolism occurs with a greater energy crisis and impairment of the normal functioning of axons and astrocytes.

Whilst downstream metabolic dysfunction has been demonstrated previously, it has mostly been limited to cellular and pre-clinical studies due to a lack of methodology to explore in vivo human based changes. Our measurements using DMI offer proof of concept of the imaging tool to be used to measure pathological changes and could offer a new method to better understand and monitor disease progression. Whilst we did not directly observe increased aerobic glycolysis through ^{2}H-Lactate changes, we observed a significant decrease in ^{2}H-Glx within the WM as EDSS score increased and lesion burden increased. This observed decrease in WM ^{2}H-Glx production is a result of the mitochondrial dysfunction that drives axonal degeneration, that is, greater as the disease progresses. As neurodegeneration occurs, owing to the failure of mitochondria in the WM to provide energy to the demyelinated axons, the axonal TCA cycle falters thereby resulting in a reduced metabolic conversion of glucose via OXPHOS into the TCA cycle to form ^{2}H-Glx. In addition to metabolic changes, axonal degeneration and loss may also play a role in the decrease of oxidative metabolic measurement with overall metabolic conversion decreased as the disease progresses. Furthermore, the fact that ^{2}H-Glc/^{2}H-Water levels remain the same across EDSS severity scales suggest that this change is not a delivery issue but instead in relation to local pathological changes.

Whilst the detection of GM is impacted by the low resolution and high voxel size of DMI, we observed a differing relationship between then WM and GM between cohorts, that changed with MS severity. Whilst in the HC, the levels of ^{2}H-Glx/^{2}H-Water were not significantly different between WM and GM, in MS the difference of oxidative metabolism differed significantly, with the difference growing as EDSS severity increased. Previous metabolic imaging studies[59] have shown that GM and WM exhibit different metabolic fluxes, with increased perfusion and downstream metabolism occurring with the GM. In comparison, our results suggest that we cannot distinguish between the cerebral metabolism using DMI at clinical field strength. This in part may be due to the low resolution and large voxel sizes of our acquisition scheme compared to other high field strength DMI studies but also may be due to the dynamics of the DMI scan, where a single timepoint offering a more steady state measure of metabolism.[60] Nonetheless, the observation of differences between the WM and GM in downstream metabolism, that increases with severity is likely to be due to cellular damage in the WM. In our MS cohort, the majority of lesions were located in the WM, suggesting that metabolic change as a result of structural damage is most likely to occur within this tissue.

Measurement of downstream metabolic changes within MS has predominately relied upon conventional proton MR spectroscopy (^{1}H-MRS), where increased levels of Glx has been seen within the NAWM and MS lesions[15] and decreases seen in grey matter regions.[14] Our measurements offer a unique perspective of metabolism within the brain providing measurement of downstream metabolism, where changes in ^{2}H-Glx reflect OXPHOS activity instead of pool sizes[61] providing a more direct insight into metabolic activity rather than that of the tightly regulated metabolic pool sizes. More recently, aerobic glycolysis was estimated using a combined FDG-PET and ASL measurement where increased levels were seen in WM reflecting the results seen in our measurements.[58]

DMI offers a novel form of imaging that can offer a unique perspective of metabolic changes with relatively low technological cost compared to methods such as FDG–PET, which present both a radiation burden to the subject and require additional scanning equipment. This study was the first to apply DMI to MS, demonstrating the potential utility this developing technology could have for measuring metabolic alterations because of neurological disease. This study applied an imaging scheme that has been used previously to show changes in Alzheimer's Disease, however, to enhance the extraction of localised information we utilised an improved post-processing reconstruction through tMPPCA denoising[25,26] and a Spectroscopy with Linear Algebraic Modelling (SLAM) reconstruction algorithm. In doing so we improved SNR to

extract useable metabolic values as well as to better differentiate tissue metabolism with the limited spatial resolution. Whilst we used 3D MRSI for our measurements, the large voxel size makes it difficult to accurately measure cerebral tissue contributions due to overlapping signals in voxels; SLAM is an extensively validated MRS technique[62,63] that has been applied to multiple nuclei for shaping, *post hoc*, the reconstructed spectral response function of spectral data from MRSI acquisitions into more analytically meaningful compartments. It essentially functions by using a higher-resolution (proton) image reference to divide spectra into *n* compartments which, subject to analytic constraints, can be mixed within each voxel in proportions determined by anatomical segmentation, as long as their overall spatial extent is comparable to multiple original MRSI voxels. SLAM therefore permits an accurate assessment of white matter versus grey matter in the brain (e.g. in proton MRS with comparable spatial resolution to our DMI acquisition[35]).[35,64,65] However, whilst this offers improved accuracy, partial volume effects still exist and our simulations of the improved SRF of the technique demonstrated that small tissue compartments, such as the CSF and lesions were not able to be accurately measured.

This pilot study had several limitations. Firstly, it is important to note the small sample size that limits the impact and generalisability of the findings. Whilst significant correlations were seen, both whole population comparisons and severity grouped comparisons lacked significant statistical power and a larger longitudinal cohort is needed to validate and confirm these results. This small MS population were all RRMS measured at one time point, with a limited range of severity (EDSS 0–6.5) and so we could not correlate changes to impairment of metabolism with progression or change of disease. Secondly, the study was limited by the inherent technical limitations of DMI at clinical field strength. The low gyromagnetic ratio limits the sensitivity of the technique and the spatial resolution able to be achieved. Whilst denoising and applying SLAM analysis enhance apparent SNR, the intrinsic challenge of DMI meant that individual lesions could not be evaluated and CSF levels could not be measured and instead the brain tissue compartments such as white matter and grey matter. Alternative methods to improve SNR such as improvements to hardware and acquisition (e.g. improved coil design[66] or balanced steady state free precession acquisition[67]) or reconstruction (e.g. further denoising strategies[68]) may offer further improvements to yield higher resolution images. Furthermore, our measurements use ^{2}H-Glc and ^{2}H-Water, both of which have overlapping spectral peaks that mean both metrics may contribute to each other's measurements. The metabolites were not corrected for T_1 values, which makes absolute quantification difficult and requires further work to obtain correct T_1 values at 3 T. In addition, the low signal strength of ^{2}H-Lactate and overlapping lipid peak means that any changes are difficult to measure, limiting our ability to measure small changes in aerobic glycolysis. As a result, increases in aerobic glycolysis due to MS progression were measured through changes in OXPHOS through ^{2}H-Glx as opposed to direct ^{2}H-Lac measurement. Alternative techniques such as hyperpolarised [1-^{13}C] pyruvate could offer improved resolution and greater sensitivity aerobic glycolysis changes to further enhance the information obtained from metabolic changes in MS.[69] Finally, whilst this study has acted as a proof of concept for DMI's capability to measure MS related downstream metabolic changes, it has not demonstrated improved capability compared to conventional methods, and therefore larger clinical imaging studies are warranted.

In summary, we have shown altered glucose metabolism in MS using DMI at clinical field strength offering a potential tool to probe the development of the disease. Through this we have shown an impairment of oxidative metabolism as disease severity increases suggesting the metabolic disruption increases as neurodegeneration progresses. These findings demonstrate the potential utility DMI may offer and supports further larger studies to validate these findings and demonstrate use as a tool to monitor MS progression.

Author contributions

Conceptualization: MV, TG, ESSH, UD, LGH, CL. Methodology: ASK, KKT, MV, TG, ESSH, UD, LGH, CL. Software: ASK, MV, ESSH, NVC, JJM, RFS. Validation: ASK, KKT, MV, NVC, JJM, LGH, CL. Formal analysis: ASK, KKT, TG, NVC, JJM, LGH, CL. Investigation: ASK, KKT, TG, CWT, UD, LGH, CL. Resources: ASK, KKT, TG, ESSH, LGH. Data curation: ASK, ESSH, LGH. Writing – original draft: ASK. Writing – review and editing: ASK, KKT, MV, TG, NVC, JJM, RFS, CWT, UD, LGH, CL. Visualization: ASK. Supervision: UD, LGH, CL. Project administration: ESSH, UD, LGH, CL. Funding acquisition: UD, LGH, CL.

Funding

The authors disclosed receipt of the following financial support for the research, authorship, and/or publication of this article: We have received funding from the Lundbeck Foundation and Novo Nordisk Foundation (NNF21OC0068683).

Declaration of conflicting interests

The authors declared the following potential conflicts of interest with respect to the research, authorship, and/or publication of this article: MV and RFS are employed by GE HealthCare.

ORCID iDs

Alixander S Khan https://orcid.org/0000-0002-9048-9553
Kamilla Kørup Trosborg https://orcid.org/0009-0004-1572-1473
Michael Vaeggemose https://orcid.org/0000-0001-7666-6819

Esben S S Hansen https://orcid.org/0000-0001-5512-9870
Nichlas Vous Christensen https://orcid.org/0000-0001-7390-6071
Jack J Miller https://orcid.org/0000-0002-6258-1299
Ulrik Dalgas https://orcid.org/0000-0003-4132-2789
Lars G Hvid https://orcid.org/0000-0003-3233-0429
Christoffer Laustsen https://orcid.org/0000-0002-0317-2911

Data availability statement

The data that support the findings of this study are available from the corresponding author upon reasonable request.

Supplemental material

Supplemental material for this article is available online.

References

1. Walton C, King R, Rechtman L, et al. Rising prevalence of multiple sclerosis worldwide: insights from the Atlas of MS. *Mult Scler* 2020; 26(14): 1816–1821.
2. McGinley MP, Goldschmidt CH and Rae-Grant AD. Diagnosis and treatment of multiple sclerosis: a review. *JAMA* 2021; 325(8): 765–779.
3. van der Weijden CW, Biondetti E, Gutmann IW, et al. Quantitative myelin imaging with MRI and PET: an overview of techniques and their validation status. *Brain* 2023; 146(4): 1243–1266.
4. Kurtzke JF. Rating neurologic impairment in multiple sclerosis: an Expanded Disability Status Scale (EDSS). *Neurology* 1983; 33(11): 1444–1452.
5. Bando Y. Mechanism of demyelination and remyelination in multiple sclerosis. *Clin Exp Neuroimmunol* 2020; 11: 14–21.
6. Rodríguez Murúa S, Farez MF and Quintana FJ. The immune response in multiple sclerosis. *Annu Rev Pathol Mech Dis* 2022; 17(1): 121–139.
7. Correale J. The role of microglial activation in disease progression. *Mult Scler* 2014; 20(10): 1288–1295.
8. Supplie LM, Düking T, Campbell G, et al. Respiration-deficient astrocytes survive as glycolytic cells in vivo. *J Neurosci* 2017; 37(16): 4231–4242.
9. de Barcelos IP, Troxell RM and Graves JS. Mitochondrial dysfunction and multiple sclerosis. *Biology* 2019; 8(2): 37.
10. Henneman DH, Altschule MD, Goncz RM, et al. Carbohydrate metabolism in brain disease: I. Glucose metabolism in multiple sclerosis. *AMA Arch Neurol Psychiatry* 1954; 72(6): 688–695.
11. Thomas AM, Barkhof F and Bulte JW. Opportunities for molecular imaging in multiple sclerosis management: linking probe to treatment. *Radiology* 2022; 303(3): 486–497.
12. De Schepper EI, Overdevest GM, Suri P, et al. Diagnosis of lumbar spinal stenosis: an updated systematic review of the accuracy of diagnostic tests. *Spine* 2013; 38(8): E469–E481.
13. Wolinsky JS, Narayana PA, Fenstermacher M, et al. Proton magnetic resonance spectroscopy in multiple sclerosis. *Neurology* 1990; 40(11): 1764–1769.
14. Chard D, Griffin C, McLean M, et al. Brain metabolite changes in cortical grey and normal-appearing white matter in clinically early relapsing–remitting multiple sclerosis. *Brain* 2002; 125(10): 2342–2352.
15. Srinivasan R, Sailasuta N, Hurd R, et al. Evidence of elevated glutamate in multiple sclerosis using magnetic resonance spectroscopy at 3 T. *Brain* 2005; 128(5): 1016–1025.
16. Paulesu E, Perani D, Fazio F, et al. Functional basis of memory impairment in multiple sclerosis: a [^{18}F] FDG PET study. *Neuroimage* 1996; 4(2): 87–96.
17. Bakshi R, Miletich RS, Kinkel PR, et al. High-resolution fluorodeoxyglucose positron emission tomography shows both global and regional cerebral hypometabolism in multiple sclerosis. *J Neuroimaging* 1998; 8(4): 228–234.
18. De Feyter HM, Behar KL, Corbin ZA, et al. Deuterium metabolic imaging (DMI) for MRI-based 3D mapping of metabolism in vivo. *Sci Adv* 2018; 4(8): eaat7314.
19. Adamson PM, Datta K, Watkins R, et al. Deuterium metabolic imaging for 3D mapping of glucose metabolism in humans with central nervous system lesions at 3T. *Magn Reson Med* 2024; 91(1): 39–50.
20. Khan AS, Peterson KA, Vittay OI, et al. Deuterium metabolic imaging of Alzheimer disease at 3-T magnetic field strength: a pilot case–control study. *Radiology* 2024; 312(1): e232407.
21. Bøgh N, Aastrup M, Mortensen JK, et al. Comparison of deuterium metabolic imaging with FDG PET in Alzheimer disease. *Radiology* 2025; 315(1): e241808.
22. McLean MA, Hinks RS, Kaggie JD, et al. Characterization and correction of center-frequency effects in X-nuclear eddy current compensations on a clinical MR system. *Magn Reson Med* 2021; 85(5): 2370–2376.
23. Schulte RF, Sacolick L, Deppe MH, et al. Transmit gain calibration for nonproton MR using the Bloch–Siegert shift. *NMR Biomed* 2011; 24(9): 1068–1072.
24. Sprenger T, Kits A, Norbeck O, et al. NeuroMix – a single-scan brain exam. *Magn Reson Med* 2022; 87(5): 2178–2193.
25. Olesen JL, Ianus A, Østergaard L, et al. Tensor denoising of multidimensional MRI data. *Magn Reson Med* 2023; 89(3): 1160–1172.
26. Christensen NV, Vaeggemose M, Bøgh N, et al. A user independent denoising method for x-nuclei MRI and MRS. *Magn Reson Med* 2023; 90(6): 2539–2556.
27. Li C, Gore JC and Davatzikos C. Multiplicative intrinsic component optimization (MICO) for MRI bias field estimation and tissue segmentation. *Magn Reson Imaging* 2014; 32(7): 913–923.
28. Purvis LA, Clarke WT, Biasiolli L, et al. OXSA: an open-source magnetic resonance spectroscopy analysis toolbox in MATLAB. *PLoS One* 2017; 12(9): e0185356.
29. Ashburner J, Barnes G, Chen C-C, et al. *SPM12 manual*, vol. 2464(4). Wellcome Trust Centre for Neuroimaging, 2014, p.53.
30. Zhang Y, Gabr RE, Schär M, et al. Magnetic resonance Spectroscopy with Linear Algebraic Modeling (SLAM) for higher speed and sensitivity. *J Magn Reson* 2012; 218: 66–76.

31. Tyler A, Lau JY, Ellis J, et al. Increased SNR and improved reproducibility for cardiac ^{31}P MRS at 7T using compartmentalized spectroscopy. In *Proceedings of the 2021 Annual Meeting of the ISMRM*, 2021; 3625.
32. Beer M, Schneider C, Köstler H, et al. *Quantitative analysis of energy metabolism in human muscle using SLOOP ^{31}P-MR-spectroscopy*. Georg Thieme Verlag, 2002, pp.573–578.
33. Bottomley PA and Zhang Y. Accelerated spatially-encoded MRS of arbitrarily-shaped compartments using linear algebraic modeling. *Handbook of magnetic resonance spectroscopy in vivo: MRS theory, practice and applications*, 2016, p.163.
34. Köstler H, Landschütz W, Koeppe S, et al. Age and gender dependence of human cardiac phosphorus metabolites determined by SLOOP ^{31}P MR spectroscopy. *Magn Reson Med* 2006; 56(4): 907–911.
35. Zhang Y, Gabr RE, Zhou J, et al. Highly-accelerated quantitative 2D and 3D localized Spectroscopy with Linear Algebraic Modeling (SLAM) and sensitivity encoding. *J Magn Reson* 2013; 237: 125–138.
36. Paul S, Christian G, Milan A, et al. An automated tool for detection of FLAIR-hyperintense white-matter lesions in multiple sclerosis. *Neuroimage* 2012; 59(4): 3774–3783.
37. Goldman MD, Marrie RA and Cohen JA. Evaluation of the six-minute walk in multiple sclerosis subjects and healthy controls. *Mult Scler* 2008; 14(3): 383–390.
38. Hochsprung A, Heredia-Camacho B, Castillo M, et al. [Clinical validity of the quantitative gait variables in patients with multiple sclerosis. A comparison of the Timed 25-foot Walk Test and the GAITRite® Electronic Walkway system]. *Rev Neurol*. 2014; 59(1): 8–12.
39. Callesen J, Richter C, Kristensen C, et al. Test–retest agreement and reliability of the Six Spot Step Test in persons with multiple sclerosis. *Mult Scler* 2019; 25(2): 286–294.
40. Bennett SE, Bromley LE, Fisher NM, et al. Validity and reliability of four clinical gait measures in patients with multiple sclerosis. *Int J MS Care* 2017; 19(5): 247–252.
41. Møller AB, Bibby BM, Skjerbæk AG, et al. Validity and variability of the 5-repetition sit-to-stand test in patients with multiple sclerosis. *Disabil Rehabil* 2012; 34(26): 2251–2258.
42. Bever C, Grattan L, Panitch H, et al. The Brief Repeatable Battery of Neuropsychological Tests for multiple sclerosis: a preliminary serial study. *Mult Scler* 1995; 1(3): 165–169.
43. Boringa JB, Lazeron RH, Reuling IE, et al. The Brief Repeatable Battery of Neuropsychological Tests: normative values allow application in multiple sclerosis clinical practice. *Mult Scler* 2001; 7(4): 263–267.
44. Fisk JD, Ritvo PG, Ross L, et al. Measuring the functional impact of fatigue: initial validation of the fatigue impact scale. *Clin Infect Dis* 1994; 18(suppl 1): S79–S83.
45. Hobart J, Lamping D, Fitzpatrick R, et al. The Multiple Sclerosis Impact Scale (MSIS-29): a new patient-based outcome measure. *Brain* 2001; 124(5): 962–973.
46. Tedeschi G, Lavorgna L, Russo P, et al. Brain atrophy and lesion load in a large population of patients with multiple sclerosis. *Neurology* 2005; 65(2): 280–285.
47. Harrison DM, Roy S, Oh J, et al. Association of cortical lesion burden on 7-T magnetic resonance imaging with cognition and disability in multiple sclerosis. *JAMA Neurol* 2015; 72(9): 1004–1012.
48. Waxman SG. Ions, energy and axonal injury: towards a molecular neurology of multiple sclerosis. *Trends Mol Med* 2006; 12(5): 192–195.
49. Smith KJ. Sodium channels and multiple sclerosis: roles in symptom production, damage and therapy. *Brain Pathol* 2007; 17(2): 230–242.
50. Kiryu-Seo S, Ohno N, Kidd GJ, et al. Demyelination increases axonal stationary mitochondrial size and the speed of axonal mitochondrial transport. *J Neurosci* 2010; 30(19): 6658–6666.
51. Fischer MT, Sharma R, Lim JL, et al. NADPH oxidase expression in active multiple sclerosis lesions in relation to oxidative tissue damage and mitochondrial injury. *Brain* 2012; 135(3): 886–899.
52. Campbell GR, Ziabreva I, Reeve AK, et al. Mitochondrial DNA deletions and neurodegeneration in multiple sclerosis. *Ann Neurol* 2011; 69(3): 481–492.
53. De Riccardis L, Rizzello A, Ferramosca A, et al. Bioenergetics profile of CD4+ T cells in relapsing remitting multiple sclerosis subjects. *J Biotechnol* 2015; 202: 31–39.
54. Campbell GR, Worrall JT and Mahad DJ. The central role of mitochondria in axonal degeneration in multiple sclerosis. *Mult Scler* 2014; 20(14): 1806–1813.
55. Rone MB, Cui Q-L, Fang J, et al. Oligodendrogliopathy in multiple sclerosis: low glycolytic metabolic rate promotes oligodendrocyte survival. *J Neurosci* 2016; 36(17): 4698–4707.
56. López-Muguruza E and Matute C. Alterations of oligodendrocyte and myelin energy metabolism in multiple sclerosis. *Int J Mol Sci* 2023; 24(16): 12912.
57. Holland R, McIntosh A, Finucane O, et al. Inflammatory microglia are glycolytic and iron retentive and typify the microglia in APP/PS1 mice. *Brain Behav Immun* 2018; 68: 183–196.
58. Brier MR, Judge B, Ying C, et al. Increased white matter aerobic glycolysis in multiple sclerosis. *Ann Neurol* 2025; 97(4): 766–778.
59. Grist JT, Miller JJ, Zaccagna F, et al. Hyperpolarized ^{13}C MRI: a novel approach for probing cerebral metabolism in health and neurological disease. *J Cereb Blood Flow Metab* 2020; 40(6): 1137–1147.
60. Kaggie JD, Khan AS, Matys T, et al. Deuterium metabolic imaging and hyperpolarized ^{13}C-MRI of the normal human brain at clinical field strength reveals differential cerebral metabolism. *Neuroimage* 2022; 257: 119284.
61. Low JCM, Wright AJ, Hesse F, et al. Metabolic imaging with deuterium labeled substrates. *Prog Nucl Magn Reson Spectrosc* 2023; 134: 39–51.
62. Bogner W, Otazo R and Henning A. Accelerated MR spectroscopic imaging – a review of current and emerging techniques. *NMR Biomed* 2021; 34(5): e4314.
63. Lee P, Adany P and Choi I-Y. Imaging based magnetic resonance spectroscopy (MRS) localization for quantitative neurochemical analysis and cerebral metabolism studies. *Anal Biochem* 2017; 529: 40–47.

64. Tyler A, Hundertmark MJ, Miller JJ, et al. Compartment-based reconstruction of acquisition-weighted ^{31}P cardiac MRSI reduces sensitivity to cardiac motion and scan planning. *Front Physiol* 2024; 14: 1325458.
65. Tyler A, Ellis J, Lau JY, et al. Compartment-based reconstruction of 3D acquisition-weighted ^{31}P cardiac magnetic resonance spectroscopic imaging at 7 T: a reproducibility study. *NMR Biomed* 2023; 36(9): e4950.
66. De Graaf RA, Hendriks AD, Klomp DWJ, et al. On the magnetic field dependence of deuterium metabolic imaging. *NMR Biomed* 2020; 33(3): e4235.
67. Iyyappan Valsala P, Pohmann R, Heule R, et al. High-resolution deuterium metabolic imaging of the human brain at 9.4 T using phase-cycled balanced SSFP spectral–spatial acquisitions. *Magn Reson Med* 2026; 95(3): 1304–1322.
68. Li Y, Zhao Y, Guo R, et al. Machine learning-enabled high-resolution dynamic deuterium MR spectroscopic imaging. *IEEE Trans Med Imaging* 2021; 40(12): 3879–3890.
69. Guglielmetti C, Najac C, Didonna A, et al. Hyperpolarized ^{13}C MR metabolic imaging can detect neuroinflammation in vivo in a multiple sclerosis murine model. *Proc Natl Acad Sci U S A* 2017; 114(33): E6982–E6991.